Received: 11 March 2024 | *Revised:* 28 April 2024 | *Accepted:* 3 May 2024
DOI: 10.37917/ijeee.22.1.14 *Vol. 22 | Issue 1 | June 2026*

Iraqi Journal for Electrical and Electronic Engineering
Original Article

Open Access
IJEEE University of Basrah College of Engineering

Comparison of methodologies For Tracking The Maximum Power Point in Fuel Cell System

Mayyadah K. Salim*, Ammar A. Aldair, Osama Y. K. Al-Atbee
Electrical Engineering Department, University of Basrah, Iraq

Correspondance
*Mayyadah K. Salim
Electrical Engineering Department
University of Basrah, Basrah, Iraq
Email: pgs.mayada.kareem@uobasrah.edu.iq

Abstract
The Maximal Power Point Tracking (MPPT) is a method employed to maximize the generated power from an energy source, such as PV (photovoltaic) or PEMFC (Proton Exchange Membrane Fuel Cell). In this study, the Grey Wolf Optimizer algorithm is utilized for the MPPT to regulate the boost converter positioned between the stack cell and the battery. The primary challenge addressed by the MPPT is that the efficiency of PEMFC is influenced by the supplied gases and cell temperature. To maintain optimal performance, the system aims to operate at the efficient power point, and the MPPT assists in achieving this by adjusting the voltage to align with the point where the PEMFC characteristic yields the maximum available power. Consequently, the MPPT's objective is to identify the Maximum Power Point (MPP) and guide the PEMFC to operate at this specific point. This process is essential to overcome challenges associated with fluctuating inputs and to optimize the system for improved performance in a PEMFC. Typically, the MPPT control algorithm involves modifying the converter duty cycle (denoted as D) to compel the PEMFCs to operate at their MPP, ensuring efficient power production even under varying input conditions

Keywords
Fuel Cell, PEMFC, FC Control.

I. Introduction

Fuel cells (FCs) are stationary electrical power generators that transform the chemical energy of fuel into electrical energy directly. FCs offer benefits such as superior efficiency, minimal or negligible emissions of pollutant gases, and a versatile modular design [1]. PEMFCs offer a source of clean energy without generating any carbon dioxide (CO2) emissions. However, if the fuel for these cells comes from fossil fuels, the fuel cells' high efficiency in internal combustion engines still results in relatively low CO2 emissions [2]. PEMFCs have become dominant in the automotive fuel cell market for various reasons. They possess specific advantages for automotive applications, including: (1) operating at an appropriately low temperature, (2) quick startup, (3) acceptable power density compared to other fuel cells, (4) durable and straightforward mechanics, (5) the ability to utilize ambient air as the oxidant, and (6) the capability to operate on pure hydrogen, consequently producing no CO2 emissions [3]. Numerous internal param-eters can influence the generated voltage of a Fuel Cell (FC). However, under any circumstance, there exists only one distinct point on the Voltage-Current (V-I) curve that represents the Maximum Power Point (MPP). At this juncture, the FC attains its highest power production. Due to the limited capacity of FC systems to generate power from the available fuel flow, it becomes essential to compel the FC to operate at the MPP. This approach helps prevent excessive fuel consumption and ensures efficient operation. A technique known as Maximum Power Point Tracking (MPPT) employs an MPPT algorithm to trace the MPP of the FC. The MPPT algorithm determines the duty cycle of a DC-DC converter, extracting a specific amount of current that corresponds to the MPP from the FC [4]. There are various techniques to

discovering the Maximum Power Point (MPP) of the optimal value of a function [5–10]. The complexity, hardware implementation, popularity, convergence speed, and sensed parameters of MPPT methods can vary [11]. A comprehensive investigation into various Maximum Power Point Tracking (MPPT) techniques, including Hill-climbing, Perturb and Observe(P&O) can be found in reference [12], incremental conductance, fractional open-circuit voltage, fractional short-circuit current, fuzzy logic control, neural network, ripple correlation control, current sweep, DC-Link capacitor droop control, load current or load voltage maximization, sliding mode control approach, and other MPPT strategies for photovoltaic systems. Several MPPT methods have been employed in fuel cells to extract the maximum available power from fuel cell modules. These methods include Perturbation and Observation(P&O) [3], adaptive MPPT control [13], Moto compressor control tech-nique [14], adaptive fuzzy logic controller [15], MPPT algorithm based on resistance matching between the internal resistance of direct methanol fuel cells and the tracker's input resistance [16] and voltage and current-based MPPT [17]. Ahmadi et al. [18] improved the PSO-based Maximum Power Point Tracking (MPPT) by incorporating a Pro-portional-Integral-Derivative(PID) controller. They subsequently employed Perturb and Observe (P&O) and Sliding Mode Control (SMC) methods to assess the results. The simulation of the PSO-PID technique exhibited superior performance, accurately tracking the maximum power point under changing conditions with precision, rapid response, and minimal power fluctuation. Derbeli et al. [19] presented an extreme seeking control (ESC) approach for achieving Maximum Power Point Tracking (MPPT) in a Proton Exchange Membrane Fuel Cell (PEMFC) system that incorporates a DC-DC boost converter. The ESC method actively monitors the Maximum Power Point (MPP) of the fuel cell during its operation, utilizing a combination of simulated and experimental data in their investigation. The findings reveal that extremum-seeking control effectively handles the fuel cell's MPP, albeit with an observed power fluctuation in the fuel cell's power output. This fluctuation poses potential risks, including damage to the PEMFC, power loss, and diminished operational efficiency. Current research trends have shifted towards intelligent optimization methods that pledge improved precision and efficiency, aiming to eradicate power fluctuations around the MPP associated with traditional techniques. In this particular study, an MPPT strategy is introduced, employing a Grey Wolf Optimizer (GWO-PI) controller designed for PEMFC systems functioning under diverse conditions such as varying temperatures, hydrogen gas pressures, and oxygen gas pressures. The proposed technique identifies the optimal operating voltage for the fuel cell system and adjusts the fuel cell operating point to maximize power by manipulating the duty cycle of the boost converter.

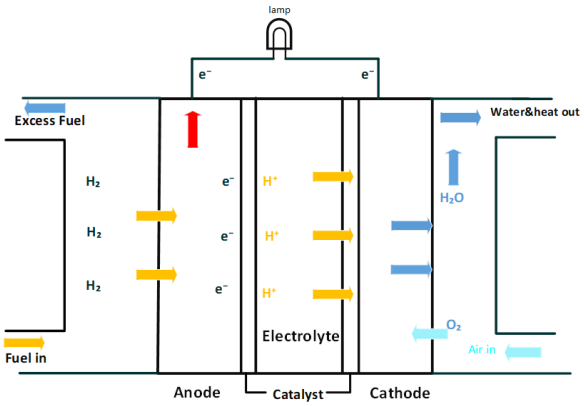

Fig. 1. The flow of charges in fuel cells

II. Problem Formulation

A. Basics of the physical operation

A fuel cell is viewed as a simple mechanism converting chemical energy into electrical energy. The construction of traditional proton Exchange membrane (PEM) fuel cells are outlined in Fig. 1, featuring two electrodes the anode and cathode with catalyst and membrane layers in between. Additionally, two channels are utilized for the supply of hydrogen and air. To illustrate the fundamental operation of fuel cells, let's consider the combustion of hydrogen based on the chemical reaction [20]

$$2H_2 + O_2 = 2H_2O + Heat + Electricity \tag{1}$$

Contrary to what was anticipated, electrical energy is generated instead of the release of heat energy. This process is elucidated as follows: On the anode side, hydrogen undergoes ionization, resulting in the release of electrons and H^+ ions in the following manner:

$$AnodeReaction : 2H_2 = 4H^+ + 4e^- \tag{2}$$

n this context, the electric energy generated is denoted by the negative electron e^-. Conversely, at the cathode, oxygen reacts with electrons sourced from the supplied air at the electrode and with H^+ ions generated by the electrolyte. Consequently, water is eventually produced as follows:

$$CathodeReaction : O_2 + 4H^+ + 4e^- = 2H_2O \tag{3}$$

B. PEM fuel cell mathematical model

A comprehensive power generation setup for Proton Exchange Membrane Fuel Cells (PEMFC) comprises a PEMFC stack, a Maximum Power Point Tracking (MPPT) controller, and a DC/DC boost converter. It is essential to investigate the mathematical modeling and characteristics of PEMFC systems. The power generation characteristics of the fuel cell exhibit nonlinearity [18]. Which is affected by factors such as cell temperature, oxygen partial pressure, hydrogen partial pressure, and membrane water content. The MATLAB Simulink model illustrating a PEMFC system is shown in Fig. 2.

Fuel cells, originally developed by Sir William Grove, have evolved into a practical energy source. In their fundamental structure, fuel cells can be likened to generators. Unlike conventional generators that employ internal combustion engines to drive an alternator, fuel cells generate electricity without relying on moving components. This lack of moving parts contributes to the reliability and efficiency of fuel cells, making them suitable for indoor use. However, fuel cells exhibit intricate and nonlinear voltage-current characteristics. As depicted in Fig. 3, a polarization curve visually represents the complex relationship between current density and voltage in a fuel cell. The voltage generated by the fuel cell is determined by the current density, which is a parameter affected by several operational variables.

Thorough mathematical models play a crucial role in fully characterizing the physical behavior, aiding in the comprehension of intricate phenomena within fuel cell systems. These models also serve as potent tools for the design and optimization of fuel cells [21]. For instance, when connecting multiple fuel cells (N_FC) in series to form a fuel cell stack system, such a model proves valuable. Engineers interested in assessing the performance of Proton Exchange Membrane Fuel Cells (PEMFC) and optimizing system parameters can benefit from

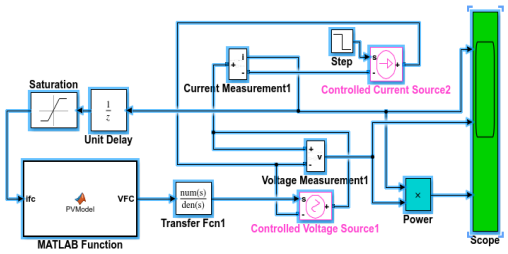

Fig. 2. The Simulink model of a PEMFC system

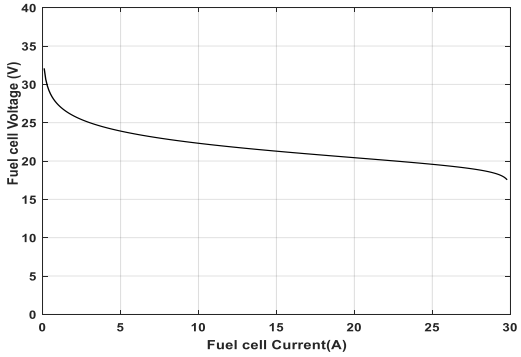

Fig. 3. PEMFC V-I polarization curve

this model. The output voltage at both ends of the battery pack terminal is typically expressed as follows:

$$V_{FC} = N_{FC}(E_{\text{Nernst}} - V_{\text{act}} - V_{\text{ohm}} - V_{\text{conc}}) \tag{4}$$

Among these factors, E_Nernst represents the reversible voltage of the fuel cell under open-circuit electrodynamic equilibrium, and its calculation is determined by using Eq. 5 [22] . V_act denotes the activation voltage drop resulting from the chemical reaction kinetics occurring around the electrode surface. This reduction leads to a steep decrease in the I-V curve of the fuel cell stack when operating at low current levels. V_ohm represents the ohmic voltage drop, which arises from the resistance encountered by positive and negative ions during electrolyte transportation. At moderate current levels, the ohmic voltage undergoes a gradual and linear reduction due to ohmic losses. V_conc denotes the concentration voltage drop, occurring in the intricate transmission process and leading to a pronounced decrease in fuel cell output voltage at higher currents [23].

$$\begin{aligned} E_{\text{Nernst}} &= 1.229 - 0.85 \times 10^{-3}(T - 298.15) + \\ &\quad 4.31 \times 10^{-5} T\,(\ln P_{H_2} + 0.5 \ln P_{O_2}) \end{aligned} \tag{5}$$

Here, T denotes the operational temperature of the fuel cell in Kelvins, $P_(H_2)$ and $P_(O_2)$ denote the partial pressures of hydrogen and oxygen, respectively. V_act is the activation voltage drop obtained from Eq. 6.

$$V_{\text{act}} = -(\zeta_1 + \zeta_2 T + \zeta_3 T \ln(C_{O_2}) + \zeta_4 T \ln(I_{FC})) \tag{6}$$

The semi-empirical coefficients are represented by $\zeta_i = 1,\ldots,4$ where $\zeta_i (i = 1-4)$ I_FC is used to signify the output

current generated by the fuel cell stack. Furthermore C_{O_2} , refers to the oxygen concentration at the cathode surface (measured in mol.cm^{-3}) and can be calculated as follows:

$$C_{O_2} = \frac{P_{o_2}}{(5.08 \times 10^6) \times \exp(-498/T)} \tag{7}$$

Ohmic loss, denoted as V_ohm, can be established through the application of Ohm's law. This calculation involves determining it as a function of current density using Eq. 8:

$$V_{\text{ohm}} = I_{FC}(R_M + R_c) \tag{8}$$

Here, R_M stands for the resistance of the membrane, and R_c represents the resistance encountered by protons as they traverse the membrane, it considered constant value according to existing literature [2, 3, 21]. Thus, the membrane surface resistance is computed in the following manner:

$$R_M = \frac{r_m t_m}{A} \tag{9}$$

In this context, t_m represents the effective thickness of the membrane surface in centimeters, while A denotes the area of the membrane's surface in square centimeters. r_m stands for the resistivity of the membrane to the flow of electrons, measured in ohm-centimeters. Empirical computations for r_m have been conducted for Nafion membrane as outlined in previous studies [2, 3, 21]:

$$r_m = \frac{181.6\left[1 + 0.03\,(I_{FC}/A) + 0.062(T/303)^2\,(I_{FC}/A)^{2.5}\,J\right.}{[\lambda_m - 0.634 - 3\,(I_{FC}/A)] \times exp(4.18(T - 303/T))} \tag{10}$$

In this context, λ_m signifies the water content of the membrane and functions as an input for the PEMFC model. Its value is dependent on the average water activity a_m, as described by the following Equation:

$$\lambda_m = \begin{cases} 0.043 + 17.81a_m - 39.85a_m^2 + 36a_m^3, 0 < a_m < 1 \\ 14 + 1.4\,(a_m - 1), \quad 1 < a_m \leq 3 \end{cases} \tag{11}$$

Eq. 12 describes the connection between the average water activity and the water vapor partial pressures at the anode and cathode, respectively.

$$a_m = \frac{1}{2}(a_{an} + a_{ca}) = \frac{1}{2}\frac{P_{v,an} + P_{v,ca}}{P_{sat}} \tag{12}$$

Equation (13) empirical formulation can be used to compute the saturation pressure of water P_sat. [24]

$$\log_{10} P_{\text{sat}} = -2.1794 + 0.02953T - 9.1813 \times 10^{-5}T^2 + 1.4454 \times 10^{-7}T^3 \tag{13}$$

The range of λ_m values is 0 to 23. The reduction in concentration voltage is put into Equation (14)

$$V_{\text{conc}} = -B \ln\left(1 - \frac{J}{J_{max}}\right) \tag{14}$$

Where B expresses the regulating parametric coefficient. J and J_max are the current density and the maximum current density (A cm–2). In order to achieve the desired voltage, fuel cells are arranged in a series configuration N_FC. This causes each individual N_FC cell within the string to exhibit nonlinear voltage-current (V-I) characteristics, as outlined in Eq. 15. In summary, determining the fuel cell output voltage involves combining the previously provided equations. It's essential to recognize that the voltage generated by a single cell is quite constrained. Therefore, a solution is to connect multiple cells to a bipolar plate to enhance the output voltage Consequently, the output voltage of the PEMFC is directly linked to the number of cells. According to Eq. 15, series cells within a string exhibit nonlinear VI properties.

$$V_{FC} = N_{FC} V_{\text{cell}} \tag{15}$$

The defined expression for the output power (W) of a PEMFC is as follows:

$$P_{FC} = V_{FC} I_{FC} \tag{16}$$

The designed system is executed in MATLAB/Simulink to assess the efficiency of the suggested MPPT approach. Following the boost converter and the MPPT method is detailed in the subsequent section.

III. DC/DC Boost Converter

The semiconductor switches play a pivotal role in a DC/DC boost converter, where the output is regulated by manipulating the duty cycle of the switching pulse provided to these switches [25]. The controller, responsible for governing the duty cycle, ensures a stable transient and steady-state response in the converter's output by regulating the pulse width and frequency of control signals supplied to the semiconductor

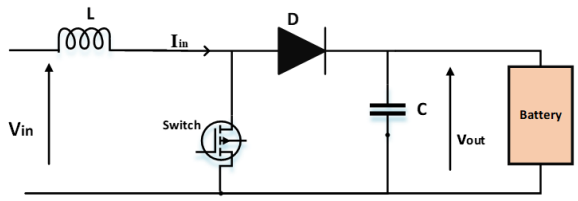

Fig. 4. DC-DC boost converter.

TABLE I.
THE SPECIFICATIONS OF THE DESIGNED CONVERTER

Description	Parameter	Nominal value
Input voltage	V_{IN}	20V
Capacitance	C	0.0668F
Inductance	L	0.0354H
Switching frequency	f_s	5000HZ
Desired output voltage	V_{OUT}	48V

switch [26, 27]. Among various contr-ollers, PID controllers are widely employed for voltage regulation in DC/DC converters due to their compatibility and flexibility in implementing specific characteristics of energy systems [28] . While PI controllers exhibit a fast res-ponse time and favorable steady-state response, transient voltage stability can be compromised. Systems with dynamic complexity and high stability requirements necessitate rob-ust controllers capable of adapting to control specific syst-ems [29]. In a power production system utilizing PEMFC, the DC/DC boost converter serves as a connection between the PEMFC and the load. It has the capability to adjust the duty cycle to align with the PEMFC Maximum Power Point (MPP), enabling the converter to modify the cell operating current and elevate the PEMFC output voltage. As shown in Fig. 4, the complete DC/DC boost converter comprises a capacitor C, an inductor L, a diode D, a load resistance R, and a switch [30]. Ensuring the availability of the necessary materials is essential for maintaining consistent production. The specifications of the designed converter are detailed in Table Fig. I

IV. MPPT TECHNIQUE

The MPPT algorithm is utilized to maximize the power output from an energy source, a crucial aspect for the efficient operation of a PEMFC power system. Given the mathematical modeling of the PEMFC, adjustments to its parameters significantly impact the power produced by the fuel cell. The key challenge addressed by the MPPT lies in the dependency of PEMFC efficiency on the supplied Partial Pressure of Reactant Gases and Cell temperature. To uphold optimal efficiency, the system must be optimized to closely align with the point where the PEMFC generates its highest available power. Consequently, the primary objective of the MPPT is to identify the Maximal Power Point (MPP) and steer the PEMFC to operate precisely at that point. This approach helps overcome challenges related to selecting the most efficient voltage, particularly when influenced by variations in input parameters. The implementation of the MPPT technique is an integral component of the PEMFC system, working in close collaboration with the DC-DC boost converter. This MPPT algorithm is essential for overseeing the switching operations of the boost converter, ensuring that the fuel cell's output voltage consistently operates at its maximum power level. When the DC-DC boost converter is connected to the PEMFC, the fuel cell's output voltage serves as the input voltage for the boost converter. Once the MPPT algorithm determines the switching status, it sends a signal to govern the boost conv-erter's switch. Consequently, the switch is either activated or deactivated based on the instructions provided by the MPPT controller. Ultimately, the boost converter maintains the fuel cell's output voltage at its peak power output. These metho-dologies aim to identify the voltage or current at which the fuel cell system provides its highest power output. In this section, we introduce an MPPT method based on Grey Wolf Optimization and Proportional-Integral (GWO-PI). Additi-onally, we explore the Grey Wolf Optimizer (GWO) and perturbation and observation (P&O) for comparison with our proposed algorithm. The subsequent subsections will prov-ide detailed descriptions of these algorithms.

A. Greywolf Optimization Algorithm

Wolves exhibit a robust hierarchy within their packs, typically organized into groups consisting of 5 to 12 wolves. [31]. Each pack is structured with a dominant wolf known as the alpha (α) wolf, followed by secondary wolves known as beta (β) wolves. Wolves subordinate to the alpha and beta wolves are referred to as delta (δ) wolves, and finally, there are follower wolves known as omega (ω) wolves. The flowchart illustrating the GWO optimization method is depicted in Fig. 5. The optimization process utilizing GWO is conducted in three primary stages, mirroring the hunting behavior of grey wolf packs in nature: encircling, hunting, and attacking.

1) Encircling stage

During this stage , every wolf adjusts its position within the search space based on the optimal position relative to the prey, which is determined by the alpha (α) wolf. Math-ematically, the encircling and corraling behaviors of the prey are modeled using Eq. 17 , Eq. 18 and Eq. 19.

$$\vec{X}(t+1) = \vec{X}_P(t) - \vec{A} \cdot \vec{D} \tag{17}$$

where $\vec{A}$, $\vec{C}$ are donated as following:

$$\vec{A} = 2\vec{a} \cdot \vec{r}_1 - \vec{a} \tag{18}$$

$$\vec{C} = 2 \cdot \vec{r}_2 \tag{19}$$

where $\vec{A}$, $\vec{D}$are coefficient vectors, $\vec{X}_P(t)$ is the prey's positions vector, $\vec{X}$mimics the position vectors of wolves, (t) is the iterations number, and $\vec{D}$ is denoted as follow:

$$\vec{D} = \left| \vec{C} \cdot \vec{X}_P(t) - \vec{X}(t) \right| \tag{20}$$

$\vec{r}_1, \vec{r}_2$ values randomly generated between zero and one, and, vector $\vec{a}$ value decreases linearly according to iterations.

2) Hunting stage

The arrangement of wolves' positions is determined by their proximity to the prey. The wolf nearest to the prey is designated as the alpha (α) wolf, while the positions of the beta (β) and delta (δ) wolves are assigned based on their distance from the prey. Eq. 20 , Eq. 21 and Eq. 22 outline the updating process for the wolves' positions.

$$\begin{aligned} \vec{X}_1 &= \vec{X}_\alpha - \vec{A}_1 \cdot \left(\vec{D}_\alpha \right), \\ \vec{X}_2 &= \vec{X}_\beta - \vec{A}_2 \cdot \left(\vec{D}_\beta \right), \\ \vec{X}_3 &= \vec{X}_\delta - \vec{A}_3 \cdot \left(\vec{D}_\delta \right) \end{aligned} \tag{21}$$

The updating positions mechanism can be calculated as follows:

$$\vec{X}(t+1) = \frac{\vec{x}_1 + \vec{X}_2 + \vec{X}_3}{3} \tag{22}$$

$$\begin{aligned} \vec{D}_\alpha &= \left| \vec{C}_1 \cdot \vec{X}_\alpha - \vec{X} \right|, \\ \vec{D}_\beta &= \left| \vec{C}_2 \cdot \vec{X}_\beta - \vec{X} \right|, \\ \vec{D}_\delta &= \left| \vec{C}_3 \cdot \vec{X}_\delta - \vec{X} \right| \end{aligned} \tag{23}$$

where $X_i\ (t+1)$ is the wolf that has the best position to the prey and i is the current iteration number of the GWO algorithm.

3) Attack stage

The assault on the prey happens when the pack is in close proximity to the prey however, prior to this, minimizing the distance between wolves and the prey is crucial. The prey represents the optimal global solution for the optimization problem. To achieve this, a vector $\vec{A}$, as defined in Eq. 18, is utilized, where a decreasing coefficient dependent on the iteration number is established. The value of vector $\vec{A}$ decreases alongside the reduction of the index value $\vec{a}$ as indicated in Eq. 21.

$$\vec{a} = 2 - t \cdot \frac{2}{t_{max}} \tag{24}$$

B. GWO with PI Techique

1) Problem formulation

The efficiency of a system is evaluated through a performance indicator. An indicator commonly employed to evaluate the performance of a PID controller facilitates the development of systems that efficiently meet the desired criteria. Control system engineers commonly use various performance metrics, with Eq. 25 offering the integral of the absolute error (IAE) performance indicator.

$$IAE = \int_0^\infty |e(t)| dt \tag{25}$$

To evaluate and improve the efficiency of systems, processes, or models, utilizing performance indices and error calculations is essential. Error calculations offer detailed insights into the accuracy and reliability of outcomes, while performance indices provide a broader evaluation of overall performance. Both are critical for making informed assessments and optimizations. The discrepancy between actual and predicted values can result in either an overestimation or underestimation, with the error typically quantified as a numerical value accompanied by a positive or negative sign. The system's capability to deliver its intended results is assessed based on the extent of discrepancy or inaccuracy observed.

2) The Procedures GWO With PI Techique

Using the Grey Wolf Optimization (GWO) technique, the following steps can be employed to fine-tune the settings of a Proportional-Integral (PI) controller for a proton exchange membrane fuel cell:

1. Define the problem clearly: Start by identifying the issue and outlining the variables requiring control. In this case, the aim is to regulate the output power of the fuel cell by optimizing the settings of the PI controller.
2. Implement the GWO algorithm: Specify parameters such

as population size, maximum number of iterations, and search range for each parameter within the GWO algorithm. This technique can be applied to optimize the PI controller settings for the PEMFC.

3. Define the objective function: Evaluate the effectiveness of the PI controller using a fitness function. Here, the controller's capability to regulate the fuel cell's output power should be quantified by the fitness function.
4. Select a PI controller: In control systems, the proportional-integral (PI) controller is commonly utilized to regulate a process variable. It acts as a feedback controller, adjusting the control signal based on the disparity between the desired setpoint and the measured process variable.
5. Specify the controller parameters: Adjust the proportional gain (Kp) and integral gain (Ki) of the PI controller. These parameters influence the controller's responsiveness and can be modified to improve the output power of the fuel cell.
6. Apply the Grey Wolf Optimization (GWO) algorithm: This population-based optimization technique is inspired by the hunting strategies of grey wolves. It serves as a metaheuristic optimization algorithm capable of finding optimal solutions to complex problems. GWO can be employed to optimize the PI controller settings for a proton exchange membrane fuel cell.
7. Execute the optimization process: Once the GWO algorithm is set up, use it to determine the optimal values of Kp and Ki for the PI controller. The GWO algorithm iterat-ively cycles through the population, adjusting the values of Kp and Ki until the fitness function is optimized.
8. Evaluate the outcomes.

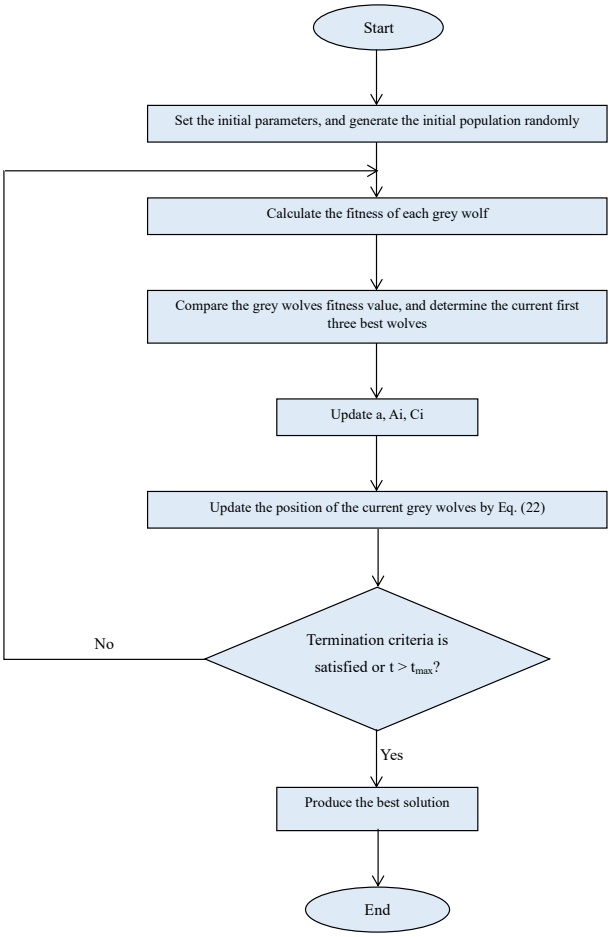

Fig. 5. The flow diagram of the GWO-based MPPT method

C. Particle Swarm Optimization

In 1995, Kennedy and Eberhart introduced a PSO algorithm [32]. which operates as a swarm intelligence technique emulating the collective behavior observed in bird swarms or fish schools in nature. The flowchart illustrating the PSO optimization method is shown in Fig. 6. In PSO, each particle is represented by a position vector and a velocity vector. These particles are distributed within a search space where one of them represents the global solution for the optimization problem. Discovering this global solution relies on evaluating and minimizing the defined objective function. Iteratively, the positions, velocities, and accelerations of particles are updated to converge towards the global solution. For each particle, a fitness function is calculated numerically. The best value obtained among all particles' fitness functions is referred to as the best global (*gbest*) value. Throughout the iteration process, each particle's best fitness function value is termed the personal best (*Pbest*). During iterations, the particles' velocities are adjusted towards the best global and personal solutions according to Eq. 26 abd Eq. 27. The position and velocity vectors are updated using the following equations.

$$V_i^{k+1} = wV_i^k + c_1 r_1 (Pbest_i^k - x_i^k) + c_2 r_2 (gbest_i^k - x_i^k) \quad (26)$$

$$X_i^{k+1} = X_i^k + V_i^{k+1} \quad (27)$$

Where v_i represents the speed update of particles, w is a factor of inertia whose value gradually decreases from 0.9 to 0.4 over time, c_1 and c_2 are coefficients of acceleration pointing towards the best global and best personal solutions, respectively. The system operates as follows [33] : The method is inspired by the behavior of swarms such as fish schools and flocks of birds. It is built on fundamental principles, requiring minimal memory usage and offering fast comp-utation.

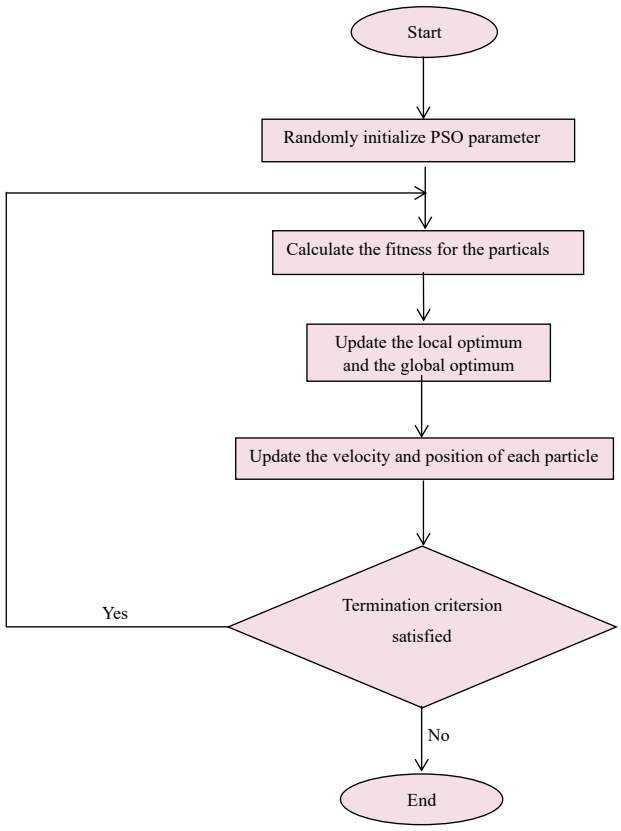

Fig. 6. The flow diagram of the PSO-based MPPT method

Initially designed for non-linear optimization problems with continuous variables, the velocity equation can express this modification, and the following equation can adjust the speed of each agent [34]. The greatest benefit of this algorithm, distinguishing it from others, is its capability for inter-particle information sharing. This exchange empowers particles to update their positions and velocities, allowing them to select the most optimal path or solution [35].

D. Perturb and Observe–Based MPPT

The 'P&O' method is a commonly employed approach by many authors and practitioners to achieve the Maximum Power Point (MPP). This method involves perturbing the voltage of the fuel cell, with the direction of the perturbation determined by the preceding power value [36]. The objective is to maintain proximity to the MPP. The basic procedure is depicted in the flowchart shown in Fig. 7. According to this diagram, if the power from the FC system increases, the adjustment in the reference voltage maintains the same direction to approach the MPP. Conversely, if the FC output power decreases, the polarity of the disturbance changes. Despite its widespread use due to its simplicity and ease of implementation, the P&O technique has limitations, especially under rapidly changing operating conditions [37]. It tends to exhibit oscillations around the MPP, particularly with larger disturbance step-sizes, and it has a relatively slow response time because of the fixed step-size utilized.

V. Simulation Results

This section involves analyzing and examining how various factors affecting the operation of a fuel cell influence its power output. Six experiments were conducted, considering different conditions such as normal operation, temperature variations, and changes in hydrogen and oxygen gas pressures. The accuracy and efficiency of the GWO-PI MPPT controller were assessed by contrasting it with alternative methods such as P&O, PSO, PSO-PI, and GWO without PI. The discussion then presents the values of observed parameters in different scenarios. The proposed MPPT method's effectiveness was tested using MATLAB /Simulink, with a system model designed for Proton Exchange Membrane Fuel Cells (PEMFC). The Simulink model, depicted in Fig. 8, illustrates the MPPT system for PEMFC. The Maximum Power Point (MPP) tracker, which connects the fuel cell system to the battery, consists of a boost dc-dc converter, GWO-MPPT, and PI controller.

A. Case1: constant operational condition

In this specific scenario, the temperature (T) is fixed at 333K, the membrane water content (λ) is set to 23, the pressure of hydrogen gas is maintained at 1 atm, and the pressure of oxygen gas is 0.2095. Fig. 9 illustrates that the GWO-PI, GWO, PSO, PSO-PI and P&O methods can all navigate around the Maximum Power Point (MPP). It is evident that P&O is responsible for power fluctuations around the MPP. In contrast, both GWO-PI and GWO effe- ctively determine the MPP, ensuring a stable output power during steady-state conditions. Moreover, GWO-PI exhibits a faster tracking speed compared to GWO. Through recurent searches for the MPP, the algorithm reveals that GWO-PI experiences fewer amplitude fluctuations than GWO, show-casing superior performance. Its quicker pace and minimal amplitude fluctuations contribute to its effectiveness comp-ared to regular GWO. The total error metric illustrates how accurately, reliably, and effectively the system operates. In situations where accuracy and reliability are paramount, the management and reduction of errors play a vital role, as illustrated in Fig. 10. The outcomes clearly indicate that GWO-PI emerges as the most favorable option. The comparison between PSO, P&O, GWO, and GWO-PI in the (MPPT) of a fuel cell involves evaluating their respective performance in optimizing the fuel cell's operation to extract the maximum available power.

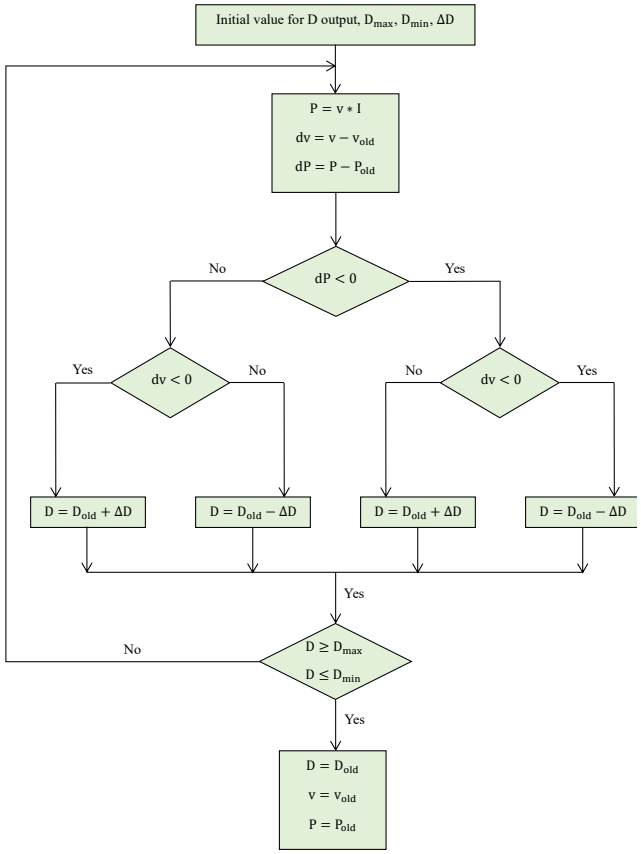

Fig. 7. The flow diagram of the P&O-based MPPT method

B. *Case 2: Variation operating condition of the temperature*

The MPPT control system is subjected to rapid fluctuations in temperature (T), considering the membrane water content 23, hydrogen gas pressure 1, and oxygen gas pressure as constant values. The objective is to evaluate the dynamic tracking capabilities of the GWO-PI algorithm Under varying operating conditions. Initially, a temperature of 303K is selected, which is then raised to 333K after 4 seconds and subsequently increased to 363K after 8 seconds. In Fig. 11, both GWO-PI and GWO demonstrate superior accuracy and stability compared to the conventional P&O method. During the search for the (MPP), GWO-PI outperforms GWO by exhibiting a higher tracking speed and fewer amplitude oscillations. The use of the P&O algorithm for MPPT, combined with optimizing control parameters through GWO or GWO-PI, proves beneficial in minimizing errors within a fuel cell system. While P&O adjusts the operating point to track maximum power, GWO and GWO-PI focus on optimizing control parameters to improve overall system performance and reduce errors, as illustrated in Fig. 12. It is clear that among the many approaches or methods being compared, the GWO-PI is superior or more effective

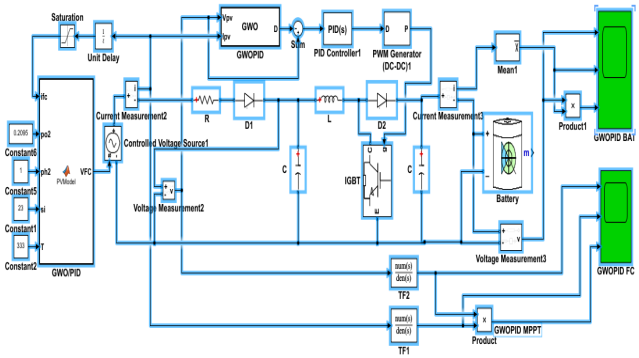

Fig. 8. GWO-PI MPPT Configuration

based on the results obtained as compared to PSO and P&O. Where GWO-PI distinguishes itself as the most successful or impactful approach among the options considered.

C. *Case 3: Variation operating condition of the hydrogen gas pressure*

The hydrogen gas pressure is a critical factor influencing the electricity generation capability of Proton Exchange Membrane Fuel Cells (PEMFC), with the temperature (T) fixed at 333K. Initially set at 0.4, the hydrogen gas pressure increases to 1 after 4 seconds and further to 1.6 at 8 seconds. In Fig. 13, the differences between various methods and their dynamic responses to changing hydrogen gas pressure are illustrated. The (P&O) approach, characterized by oscillation around (MPP), leads to more significant power losses and potential harm to the fuel cell, as indicated by the data. Contrastingly, the GWO-PI method shows less amplitude oscillations than GWO. Moreover, GWO-PI exhibits a hig-her convergence speed and less amplitude oscillation during the search process compared to GWO. The increase in hyd-rogen gas pressure supplied to the fuel cell corresponds to an elevated power output from the fuel cell. The GWO-PI algorithm plays a crucial role in reducing the total error in fuel cell power by utilizing the GWO optimization process to fine-tune the parameters of (PI) controller. This integration enhances the control system's ability to regulate fuel cell power output, leading to improved performance and minimized errors, as depicted in Fig. 14. The results make it clear that GWO-PI is the most effective approach in this context as compared to PSO and P&O.

D. *Case 4: Variation operating condition of the oxygen gas pressure*

The pressure of oxygen gas plays a crucial role in influencing the output power and overall performance of a fuel cell. Initially set at 0.1095, the oxygen gas pressure increases to 0.2095 at 4 seconds and further to 0.3095 at 8 seconds. Higher oxygen pressure enhances the availability of reactant

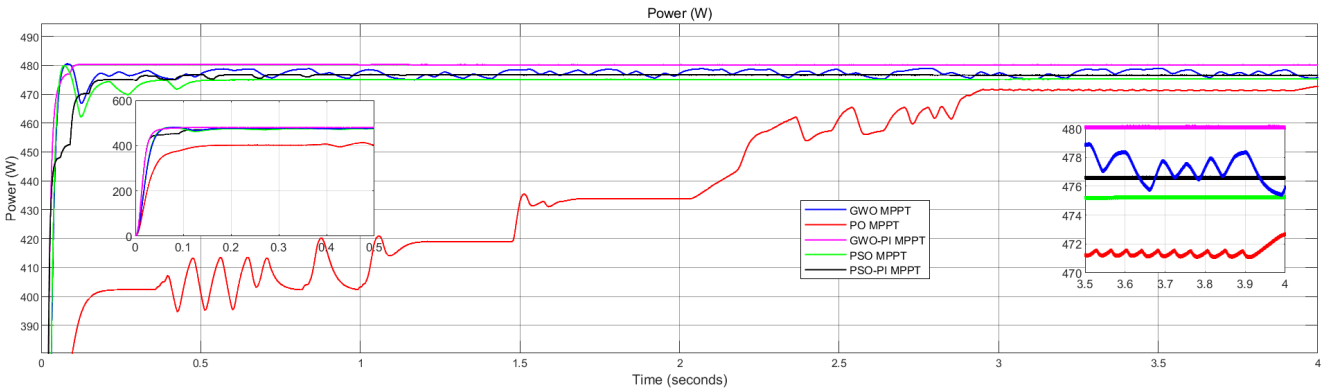

Fig. 9. MPPT under constant operational condition

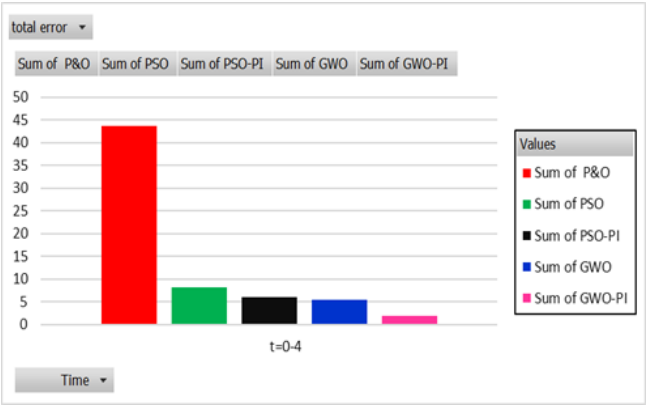

Fig. 10. Total error of MPPT under constant operational condition.

molecules at the cathode, thereby accelerating electrochemical reactions and generally leading to an increased power output. This effect is illustrated in Fig. 15. In comparison to the conventional (P&O) method, both GWO-PI and GWO exhibit superior accuracy and stability. During the search for the (MPP), GWO-PI outperforms GWO by demonstrating a higher tracking speed and less amplitude oscillation. In the context of a fuel cell system, the term ”total error” encompasses cumulative errors, inaccu-racies, or deviations that may occur during system operation or control. These errors can arise from fluctuations in operating conditions or limitations in the control algorithms employed to regulate the system. Managing and reducing total error is critical for ensuring the reliable and efficient performance of the fuel cell system, as highlighted in Fig. 16. The results make it clear that GWO-PI stands out as the optimal choice in this scenario as compared to PSO and P&O.

E. Case 5: Variation operating condition of the hydrogen and oxygen gas Pressure

The hydrogen gas pressure initiates at 0.4 and increases to 1 after 4 seconds, then further rises to 1.6 at 8 seconds. Simultaneously, the oxygen gas pressure begins at 0.1095, elevates to 0.2095 at 4 seconds, and increases again to 0.3095 at 8 seconds. In Fig. 17, the variations between different methods and their dynamic responses to changing hydrogen and oxygen gas pressures are depicted. The (P&O) appr-oach, characterized by oscillations around the (MPP), results in more significant power losses and potential harm to the fuel cell, according to the presented statistics. In contrast, the GWO-PI method demonstrates fewer amplitude oscillations than GWO. Moreover, GWO-PI exhibits a higher conver-gence speed and less amplitude oscillation throughout the search process compared to GWO. The increase in pressure for both hydrogen and oxygen gases supplied to the fuel cell correlates with an elevated power output from the fuel cell. The GWO-PI algorithm plays a crucial role in error reduction within a control system by integrating the GWO algorithm with a (PI) controller. This integration optimizes the PI parameters, leading to improved adaptability and reduced discrepancies between the desired and actual system responses, as shown in Fig. 18. The results make it evident that GWO-PI is the most effective approach in this context.

F. Case 6: Variation operating condition of the Temperature, hydrogen and oxygen gases pressure

Temperature, hydrogen pressure, and oxygen gas pres-sure collectively influence the efficiency of Proton Exchange Membrane (PEM) fuel cells. The fuel cell’s voltage and current output show an upward trend with increasing values of oxygen gas pressure, hydrogen gas pressure, and temperature. The initial temperature is set at 303K, which is then raised to 333K after 4 seconds and further increased to 363K at 8 seconds. Simultaneously, the hydrogen gas pressure starts at

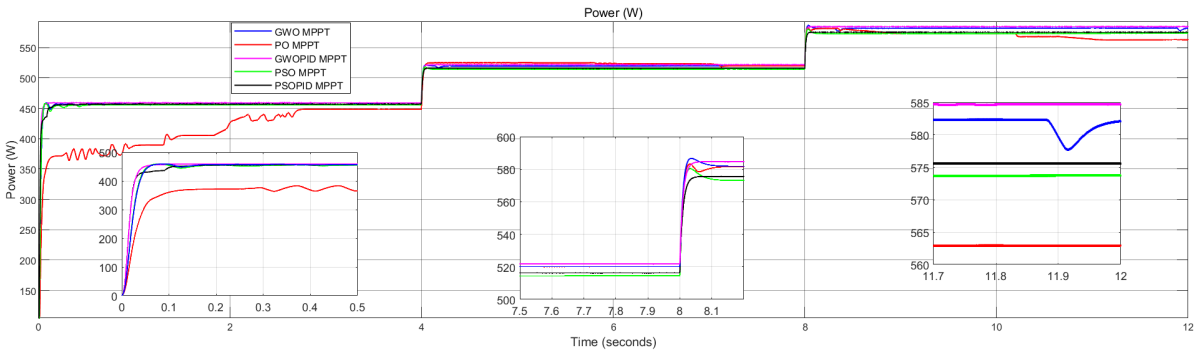

Fig. 11. MPPT under Variation operating condition of the temperature

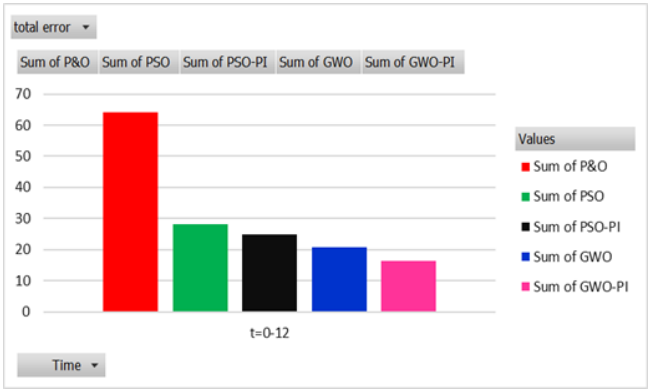

Fig. 12. Total error of MPPT under Variation operating condition of the temperature

0.4, increases to 1 after 4 seconds, and further climbs to 1.6 at 8 seconds. The oxygen gas pressure, initially at 0.3095, decreases to 0.2095 at 4 seconds and further to 0.1095 at 8 seconds. In Fig. 19, it is GWO and P&O methods. P&O exhibits a slow time response and notable power fluctuations near the Maximum Power Point (MPP). In contrast, GWO exhibits reduced power fluct-uations and improved time response compared to P&O while tracking the MPP. The GWO-PI algorithm achieves a comprehensive reduction in errors by merging the GWO process with a (PI) controller. This integration optimizes the PI parameters, enhancing system adaptability for improved regulation and minimized errors over time, as illustrated in Fig. 20. The results clearly demonstrate that GWO-PI stands out as the most effective approach in this context.

VI. Conclusion

A study focused on enhancing the power capacity of Proton Exchange Membrane Fuel Cells (PEMFCs) by introducing a Maximum Power Point Tracking (MPPT) controller. The operating conditions of PEMFCs significantly influence their characteristic curve, particularly affec-ting the Maximum Power Point (MPP). The MPP represents the point at which the fuel cell operates most efficiently in terms of power generation. To address this, the study proposes the integration of a MPPT controller based on GWO with (PI) control. This controller aims to dynamically track the MPP under changing operating conditions, such as variations in temperature and gas pressure. To evaluate the effectiveness of the proposed GWO-PI controller, a simulation model is built using MATLAB/Simulink. The GWO-PI controller is compared against two other methods: PSO and Perturb and Observe (P&O), which is a commonly used MPPT algo-rithm. Six different scenarios are considered in the eval-uation, including fixed operating conditions and changing conditions for temperature and gas pressure. The results demonstrate that the GWO-PI controller outperforms both P&O and PSO in terms of tracking speed and amplitude oscillation. This implies that the GWO-PI controller can more effectively adapt to changes in operating conditions and optimize the fuel cell's output power. Additionally, the GWO-PI algorithm is found to be more efficient in optimizing the PI parameters, leading to reduced errors in fuel cell power output compared to the other methods. The study suggests that GWO with PI control for MPPT in PEMFCs can enhance their power capacity by effectively tracking the MPP under varying operating conditions, thereby improving overall performance and stability.

Conflict of Interest

The authors have no conflict of relevant interest to this article.

References

[1] D. Akinyele, E. Olabode, and A. Amole, "Review of fuel cell technologies and applications for sustainable microgrid systems," *Inventions*, vol. 5, no. 3, p. 42, 2020.

[2] A. A. Z. Diab, H. Ali, H. Abdul-Ghaffar, H. A. Abdelsalam, and M. Abd El Sattar, "Accurate parameters

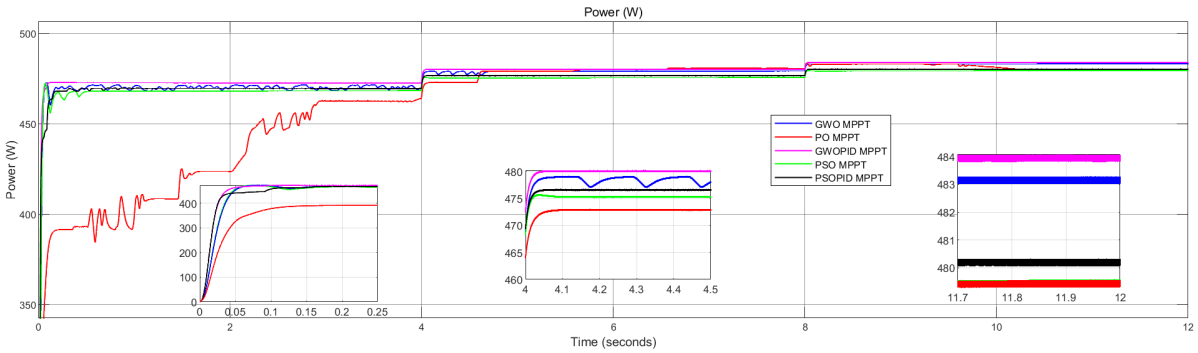

Fig. 13. MPPT under Variation operating condition of the hydrogen gas pressure.

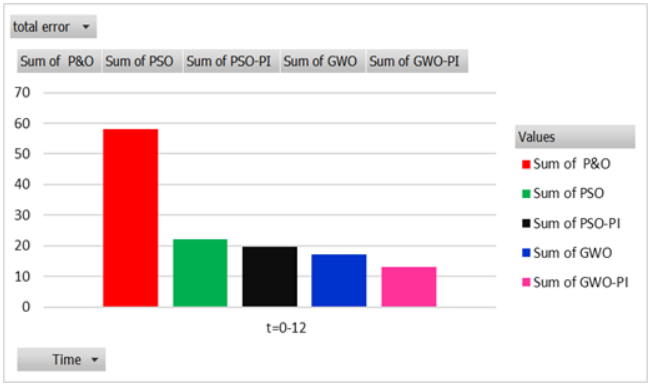

Fig. 14. Total error of MPPT under Variation operating condition of the hydrogen gas pressure

extraction of pemfc model based on metaheuristics algorithms," *Energy Reports*, vol. 7, pp. 6854–6867, 2021.

[3] M. A. Mossa, O. M. Kamel, H. M. Sultan, and A. A. Z. Diab, "Parameter estimation of pemfc model based on harris hawks' optimization and atom search optimization algorithms," *Neural Computing and Applications*, vol. 33, pp. 5555–5570, 2021.

[4] H. Islam, S. Mekhilef, N. B. M. Shah, T. K. Soon, M. Seyedmahmousian, B. Horan, and A. Stojcevski, "Performance evaluation of maximum power point tracking approaches and photovoltaic systems," *Energies*, vol. 11, no. 2, p. 365, 2018.

[5] N. Naseri, S. El Hani, A. Aghmadi, K. El Harouri, M. S. Heyine, and H. Mediouni, "Proton exchange membrane fuel cell modelling and power control by p&o algorithm," in *2018 6th International Renewable and Sustainable Energy Conference (IRSEC)*, pp. 1–5, IEEE, 2018.

[6] M. H. Wang, M.-L. Huang, W.-J. Jiang, and K.-J. Liou, "Maximum power point tracking control method for proton exchange membrane fuel cell," *IET Renewable Power Generation*, vol. 10, no. 7, pp. 908–915, 2016.

[7] N. Karami, L. El Khoury, G. Khoury, and N. Moubayed, "Comparative study between p&o and incremental conductance for fuel cell mppt," in *International conference on renewable energies for developing countries 2014*, pp. 17–22, IEEE, 2014.

[8] D. N. Luta and A. K. Raji, "Fuzzy rule-based and particle swarm optimisation mppt techniques for a fuel cell stack," *Energies*, vol. 12, no. 5, p. 936, 2019.

[9] J. Jiao and X. Cui, "Adaptive control of mppt for fuel cell power system," *J. Converg. Inf. Technol*, vol. 8, no. 4, pp. 362–371, 2013.

[10] K. Afshar, N. Bigdeli, and S. Ahmadi, "A novel approach for robust maximum power point tracking of pem fuel cell generator using sliding mode control approach," *International Journal of Electrochemical Science*, vol. 7, no. 5, pp. 4192–4209, 2012.

[11] A. O. Baba, G. Liu, and X. Chen, "Classification and evaluation review of maximum power point tracking methods," *Sustainable Futures*, vol. 2, p. 100020, 2020.

[12] P. Motsoeneng, J. Bamukunde, and S. Chowdhury, "Comparison of perturb & observe and hill climbing mppt schemes for pv plant under cloud cover and varying load," in *2019 10th International Renewable Energy Congress (IREC)*, pp. 1–6, IEEE, 2019.

[13] S. Hosseini, S. Danyali, F. Nejabatkhah, and S. K. M. Niapoor, "Multi-input dc boost converter for grid connected hybrid pv/fc/battery power system," in *2010 IEEE Electrical Power & Energy Conference*, pp. 1–6, IEEE, 2010.

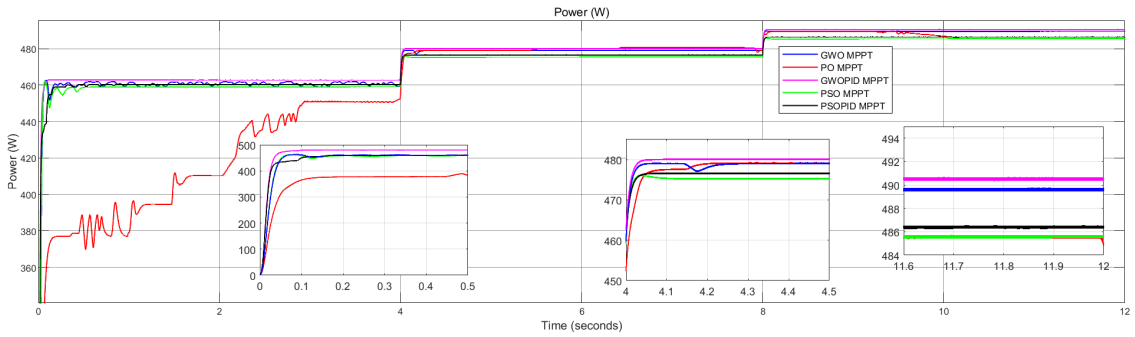

Fig. 15. MPPT under Variation operating condition of the oxygen gas pressure.

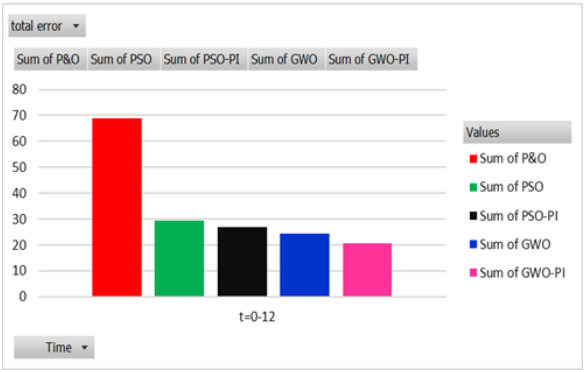

Fig. 16. Total error of MPPT under Variation operating condition of the oxygen gas pressure.

[14] M. Becherif and D. Hissel, "Mppt of a pemfc based on air supply control of the motocompressor group," *International Journal of Hydrogen Energy*, vol. 35, no. 22, pp. 12521–12530, 2010.

[15] N. Chanasut and S. Premrudeepreechacharn, "Maximum power control of grid-connected solid oxide fuel cell system using adaptive fuzzy logic controller," in *2008 IEEE Industry Applications Society Annual Meeting*, pp. 1–6, IEEE, 2008.

[16] K. H. Loo, G. Zhu, Y. Lai, and K. T. Chi, "Development of a maximum-power-point tracking algorithm for direct methanol fuel cell and its realization in a fuel cell/supercapacitor hybrid energy system," in *8th International Conference on Power Electronics-ECCE Asia*, pp. 1753–1760, IEEE, 2011.

[17] M. Sarvi and M. Barati, "Voltage and current based mppt of fuel cells under variable temperature conditions," in *45th International Universities Power Engineering Conference UPEC2010*, pp. 1–4, IEEE, 2010.

[18] S. Ahmadi, S. Abdi, and M. Kakavand, "Maximum power point tracking of a proton exchange membrane fuel cell system using pso-pid controller," *International journal of hydrogen energy*, vol. 42, no. 32, pp. 20430–20443, 2017.

[19] M. Derbeli, O. Barambones, M. Y. Silaa, and C. Napole, "Real-time implementation of a new mppt control method for a dc-dc boost converter used in a pem fuel cell power system," in *Actuators*, vol. 9, p. 105, MDPI, 2020.

[20] Z.-J. Mo, X.-J. Zhu, L.-Y. Wei, and G.-Y. Cao, "Parameter optimization for a pemfc model with a hybrid genetic algorithm," *International Journal of Energy Research*, vol. 30, no. 8, pp. 585–597, 2006.

[21] J. C. Amphlett, R. Baumert, R. F. Mann, B. A. Peppley, P. R. Roberge, and T. J. Harris, "Performance modeling of the ballard mark iv solid polymer electrolyte fuel cell: Ii. empirical model development," *Journal of the Electrochemical Society*, vol. 142, no. 1, p. 9, 1995.

[22] O. E. Turgut and M. T. Coban, "Optimal proton exchange membrane fuel cell modelling based on hybrid teaching learning based optimization–differential evolution algorithm," *Ain Shams Engineering Journal*, vol. 7, no. 1, pp. 347–360, 2016.

[23] R. F. Mann, J. C. Amphlett, M. A. Hooper, H. M. Jensen, B. A. Peppley, and P. R. Roberge, "Development and application of a generalised steady-state electrochemical model for a pem fuel cell," *Journal of power sources*, vol. 86, no. 1-2, pp. 173–180, 2000.

[24] Y. Chen and N. Wang, "Cuckoo search algorithm with explosion operator for modeling proton exchange membrane fuel cells," *International Journal of Hydrogen Energy*, vol. 44, no. 5, pp. 3075–3087, 2019.

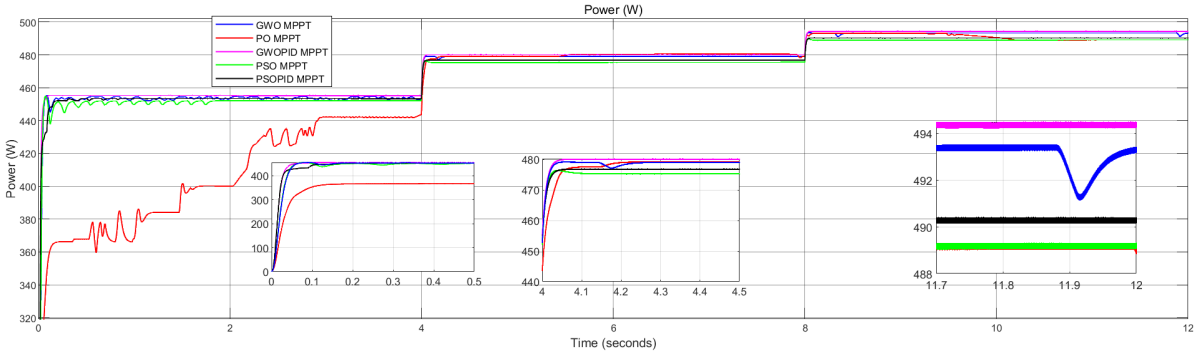

Fig. 17. MPPT under Variation operating condition of the hydrogen and oxygen gas pressure

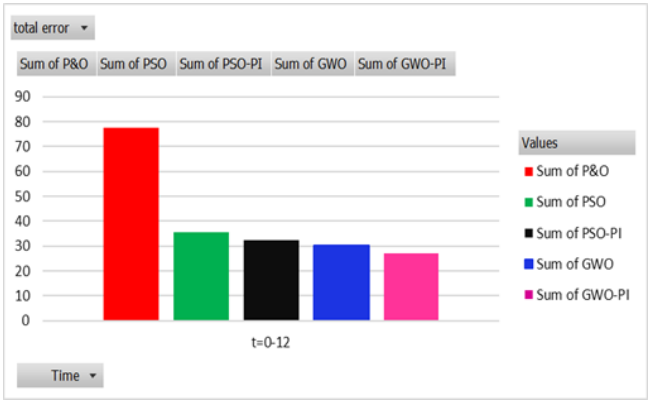

Fig. 18. Total error of MPPT under Variation operating condition of the hydrogen and oxygen gas pressure

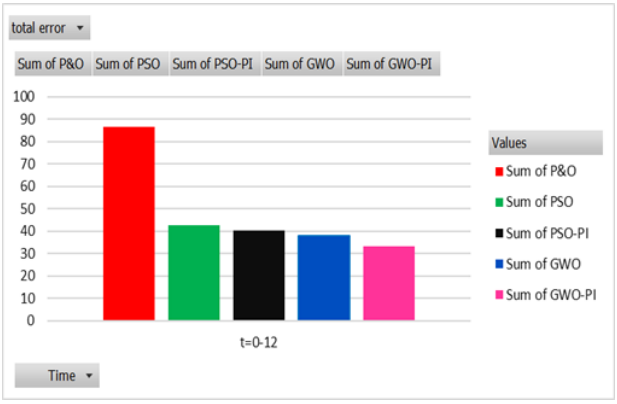

Fig. 20. Total error of MPPT under Variation operating condition of the Temperature, hydrogen and oxygen gases pressure.

[25] A. Marahatta, Y. Rajbhandari, A. Shrestha, A. Singh, A. Gachhadar, and A. Thapa, "Priority-based low voltage dc microgrid system for rural electrification," *Energy Reports*, vol. 7, pp. 43–51, 2021.

[26] S. Saadatmand, P. Shamsi, and M. Ferdowsi, "The voltage regulation of a buck converter using a neural network predictive controller," in *2020 IEEE Texas Power and Energy Conference (TPEC)*, pp. 1–6, IEEE, 2020.

[27] M. S. Alam, F. S. Al-Ismail, A. Salem, and M. A. Abido, "High-level penetration of renewable energy sources into grid utility: Challenges and solutions," *IEEE access*, vol. 8, pp. 190277–190299, 2020.

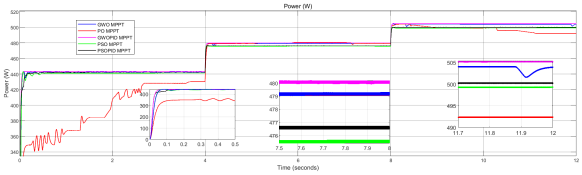

Fig. 19. MPPT under Variation operating condition of the Temperature, hydrogen and oxygen gases pressure

[28] M. Islam, A. F. Abdul Ghaffar, E. Sulaeman, M. M. Ahsan, A. Z. Kouzani, and M. P. Mahmud, "Performance analysis of pi and dmrac algorithm in buck–boost converter for voltage tracking in electric vehicle using simulation," *Electronics*, vol. 10, no. 20, p. 2516, 2021.

[29] C. Cui, N. Yan, and C. Zhang, "An intelligent control strategy for buck dc-dc converter via deep reinforcement learning," *arXiv preprint arXiv:2008.04542*, 2020.

[30] R. Abdul-Halem, H. A. Hairik, and A. J. Kadhem, "Experimental prototype for pwm-based sliding mode boost converter," in *2010 1st International Conference on Energy, Power and Control (EPC-IQ)*, pp. 230–236, IEEE, 2010.

[31] S. Mirjalili, S. M. Mirjalili, and A. Lewis, "Grey wolf optimizer adv eng softw 69: 46–61," *ed*, 2014.

[32] J. Kennedy and R. Eberhart, "Particle swarm optimization," in *Proceedings of ICNN'95-international conference on neural networks*, vol. 4, pp. 1942–1948, ieee, 1995.

[33] I. A. Amin, D. Y. Mahmood, and A. H. Numan, "Optimal localization of upfc for transmission line losses minimizing using particle swarm optimization," *Engineering and Technology Journal*, vol. 39, no. 10, pp. 1463–1472, 2021.

[34] F. S. Abdulla, A. N. Hamoodi, and A. M. Kheder, "Particle swarm optimization algorithm for solar pv system under partial shading.," *Przeglad Elektrotechniczny*, vol. 97, no. 10, 2021.

[35] B. N. A. Samed and A. A. Aldair, "Design tunable robust controllers for unmanned aerial vehicle based on particle swarm optimization algorithm.," *Iraqi Journal for Electrical & Electronic Engineering*, vol. 15, no. 2, 2019.

[36] F. Liu, Y. Kang, Y. Zhang, and S. Duan, "Comparison of p&o and hill climbing mppt methods for grid-connected pv converter," in *2008 3rd IEEE Conference on Industrial Electronics and Applications*, pp. 804–807, IEEE, 2008.

[37] M. A. G. De Brito, L. Galotto, L. P. Sampaio, G. d. A. e Melo, and C. A. Canesin, "Evaluation of the main mppt techniques for photovoltaic applications," *IEEE transactions on industrial electronics*, vol. 60, no. 3, pp. 1156–1167, 2012.